THE OXIDATION OF CARBON MONOXIDE ON Rh(100) UNDER STEADY STATE CONDITIONS: AN FT-IR STUDY

Lam-Wing H. LEUNG and D. Wayne GOODMAN

Department of Chemistry, Texas A&M University, College Station, TX 77843-3255, U.S.A.

Received 26 February 1990; accepted 14 May 1990

Carbon monoxide oxidation on Rh(100), infrared reflection absorption spectroscopy (IRAS), quadrupole mass spectrometry, low energy electron diffraction (LEED), Auger electron spectroscopy (AES), FTIR spectrometry, ultrahigh vacuum (UHV) system.

The steady-state oxidation of CO on clean Rh(100) at low pressures has been investigated using in-situ infrared spectroscopy and mass spectrometry. The results show that at a fixed CO pressure, the temperature at which the CO_2 formation rate maximizes decreases as a function of increasing O_2 pressure. Vibrational data indicate that this maximum rate coincides with a CO coverage of less than 0.01 monolayers.

1. Introduction

The oxidation of carbon monoxide by oxygen over noble metal catalysts has been a subject of considerable interest [1,2]. Recent investigations of this reaction on polycrystalline [3–5] and single crystal [6,7] rhodium surfaces at low pressures have led to a more complete understanding of the reaction mechanism and kinetics as well as the role of adsorbed carbon monoxide and oxygen in this important reaction. While most studies thus far have provided valuable kinetic information, the examination of the nature of adsorbed CO during reaction is of particular interest. In this study we have employed infrared reflection absorption spectroscopy (IRAS) to obtain vibrational spectra of CO during steady-state oxidation of CO on Rh(100) at low pressures ($\leq 10^{-7}$ Torr). Here we will discuss the temperature-dependent infrared spectra for CO adsorbed on Rh(100) over a range of CO and O_2 gas-phase compositions. We also will discuss the relationship between the vibrational properties of adsorbed CO on Rh(100) and the CO_2 formation rate under identical steady-state CO oxidation conditions.

2. Experimental section

All experiments were carried out in an ultrahigh vacuum (UHV) system equipped with quadrupole mass spectrometry, low-energy electron diffraction

(LEED), and Auger electron spectroscopy (AES), coupled to a commercial FTIR spectrometer (Mattson Instruments, Inc.). The vacuum chamber, equipped with turbomolecular and titanium sublimation pumps, achieved base pressures of $\sim 2 \times 10^{-10}$ Torr. A full description of this apparatus will be given elsewhere [8].

The Rh(100) sample consisted of a disc ~ 1 cm in diameter and was heated resistively by tungsten leads spot-welded to the rear of the crystal. Temperature measurement was made by a chromel-alumel thermocouple spot-welded to the back side of the sample. The crystal was cleaned by a combination of O_2 and H_2 treatment [9] followed by annealing at ~ 1200 K for 5 minutes. AES showed no detectable amount of sulfur, boron, or carbon.

The IRAS experiments were performed with a Mattson Cygnus 100 spectrometer slightly modified so that the collimated IR beam was focused onto the crystal at an angle of incidence of 85° and was then recollimated and focused onto a liquid nitrogen cooled mercury cadmium telluride (MCT) detector. All IRAS spectra reported here were obtained with the spectrometer operating at 4 cm^{-1} resolution by typically adding 500 interferometer scans (4 minutes) and were then ratioed against a stored background spectrum of the clean surface.

A typical experiment was carried out by first cleaning the sample followed by acquiring a background spectrum. CO and O_2 of research purity (Matheson) were then introduced into the UHV chamber through two separate leak valves to the desired partial pressures, and the IRAS spectra were recorded with the sample heated to various temperatures. The rate of CO_2 formation was measured under identical conditions with a calibrated quadrupole mass spectrometer. Since the system was continuously pumped, the increase in CO_2 pressure above background is proportional to the CO_2 formation rate.

3. Results and discussion

Figure 1A displays a series of temperature-dependent infrared spectra obtained during exposure of an initially clean Rh(100) crystal to a background CO pressure of 1×10^{-7} Torr. Similar to recent EELS studies [9,10] of CO absorbed on Rh(100), both linear and bridged CO are formed upon adsorption on Rh(100) as indicated by IR bands at 1990–2070 cm^{-1} and 1875–1950 cm^{-1}, respectively. As shown in fig. 1A, the peak frequency of both the linear and bridged CO bands decreases as a function of increased crystal temperature. This can be explained in part by CO desorption from the Rh(100) surface at temperatures above 350 K [9–12] which leads to decreasing CO coverage, thereby resulting in less vibrational coupling within the CO adsorbed layer. The reduction in CO coverage is apparent from the decrease in absorption intensity of the CO bands in this temperature region. At temperatures below that of significant CO desorption ($T \leq 350$ K), a downshift in peak frequency with increased temperature can be rationalized using the vibrational dephasing model described by Persson, et al.

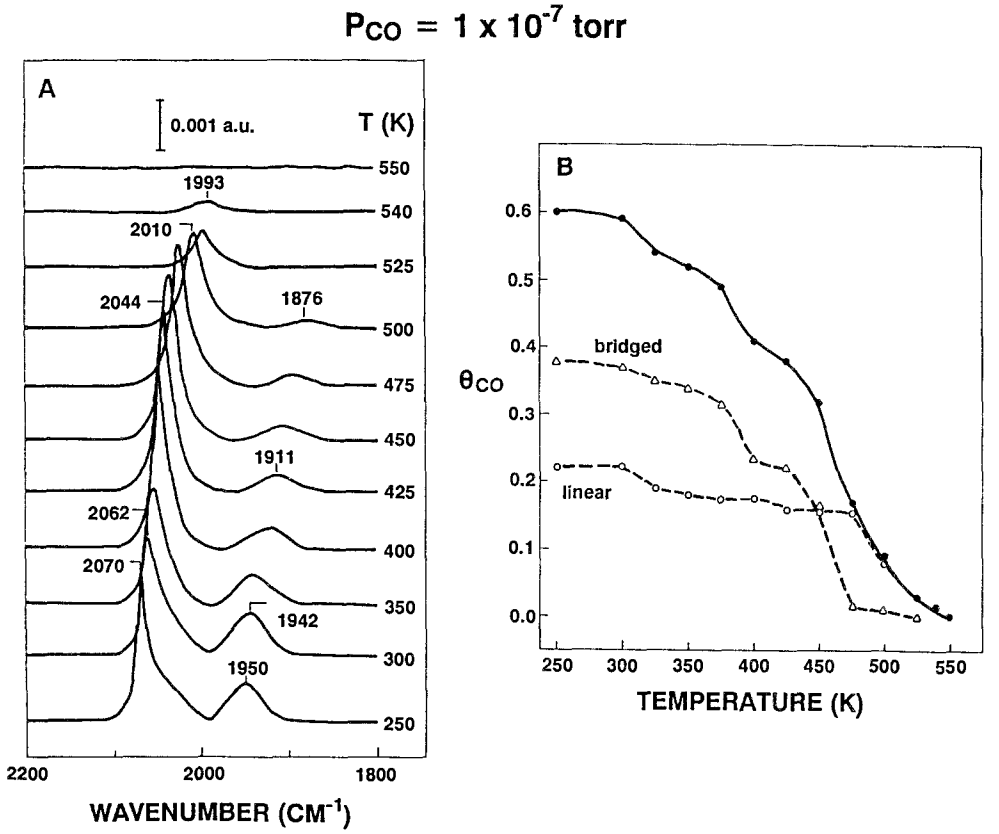

Fig. 1. (A) Vibrational spectra in the C–O stretch region for CO (1×10^{-7} Torr) on Rh(100) as a function of increasing temperature as indicated. (B) Plots of overall CO coverages (filled circles), linear CO coverages (open circles) and bridged CO coverages (open triangles) versus temperature during exposure to 1×10^{-7} Torr CO.

[13]. In this model, the high frequency C–O stretching mode is anharmonically coupled to a thermally excited low frequency mode.

A binding energy difference of 0.3 kcal mol^{-1} between linear (less stable) and bridged CO species has been determined from our recent IRAS studies of CO adsorption on Rh(100) [8]. In addition, we have estimated the ratio of the dynamic dipole moments for the linear and bridged CO IR bands, (e_l^*/e_b^*), to be 4.0 ± 0.5 [8]. Taking into account the variation of integrated absorption intensity of both the linear and bridged IR bands as a function of CO coverage [8] and the ratio of the dynamic dipole moments for these two states, we have determined the CO coverage and the populations of the linear and bridged CO species as a function of temperature. The resulting plots of the overall CO coverage (filled circles), the amount of linear CO species (open circles) and that of bridged CO species (open triangles) versus temperature for 1×10^{-7} Torr CO are shown in fig. 1B. The saturation coverage of CO on Rh(100) at 100 K is approximately 0.75

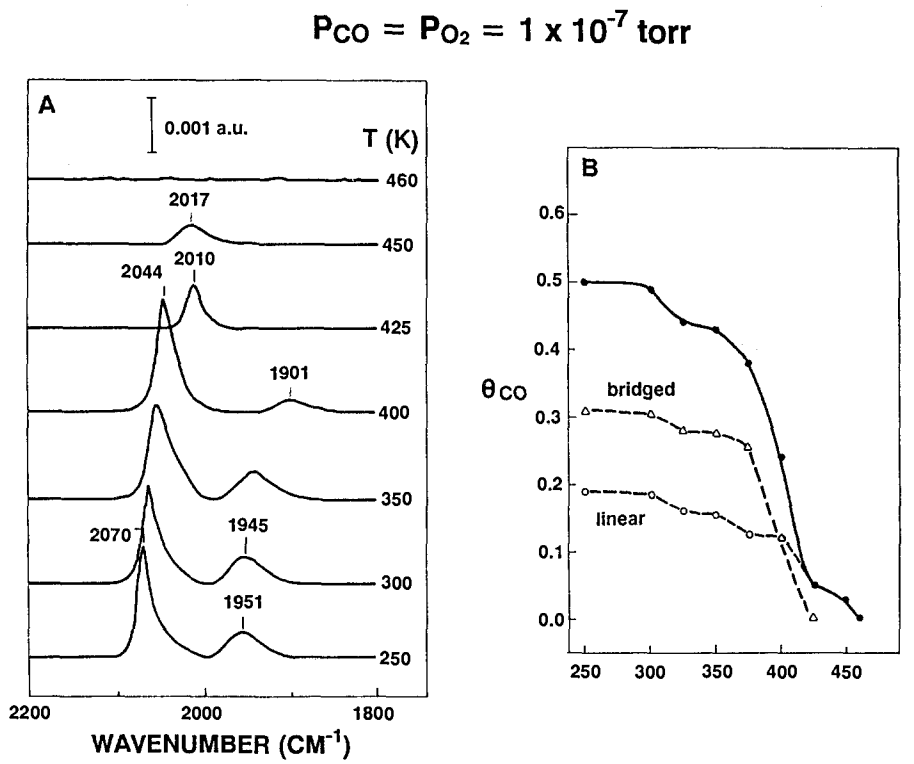

Fig. 2. (A) Vibrational spectra in the C–O stretch region during steady-state reaction with $P(CO) = P(O_2) = 1 \times 10^{-7}$ Torr. (B) Plots of overall CO coverages (filled circles), linear CO coverages (open circles) and bridged CO coverages (open triangles) versus temperature during steady-state reaction with $P(CO) = P(O_2) = 1 \times 10^{-7}$ Torr.

ML [8]; however, due to the partial CO desorption at temperature above 200 K, we have estimated a saturation CO coverage of ~ 0.6 ML at 250 K as indicated in fig. 1B. As shown in fig. 1B, at temperatures below 450 K, the bridged CO species is present as the preferred orientation while the amount of linear CO species remains virtually constant until approximately 475 K. At this temperature the CO desorption rate becomes substantial.

Infrared spectra similar to that shown in fig. 1A were also obtained during exposure of a clean Rh(100) crystal to a mixture of CO and O_2. Representative IR spectra obtained at the indicated temperatures with 1×10^{-7} Torr CO and 1×10^{-7} Torr O_2 are shown in fig. 2A. In general, both the peak frequency and the lineshape of these spectra (fig. 2A) at temperatures below 350 K are similar to the spectra shown in fig. 1A. The overall CO coverage and the populations of both the linear and bridged CO species versus temperature are shown in fig. 2B for 1×10^{-7} Torr CO and 1×10^{-7} Torr O_2. It is noteworthy that θ_{CO}–T plots similar to that displayed in figs. 1B and 2B have been reported for Rh(111) surfaces where the total CO coverage was determined by X-ray photoelectron spectroscopy (XPS) [7].

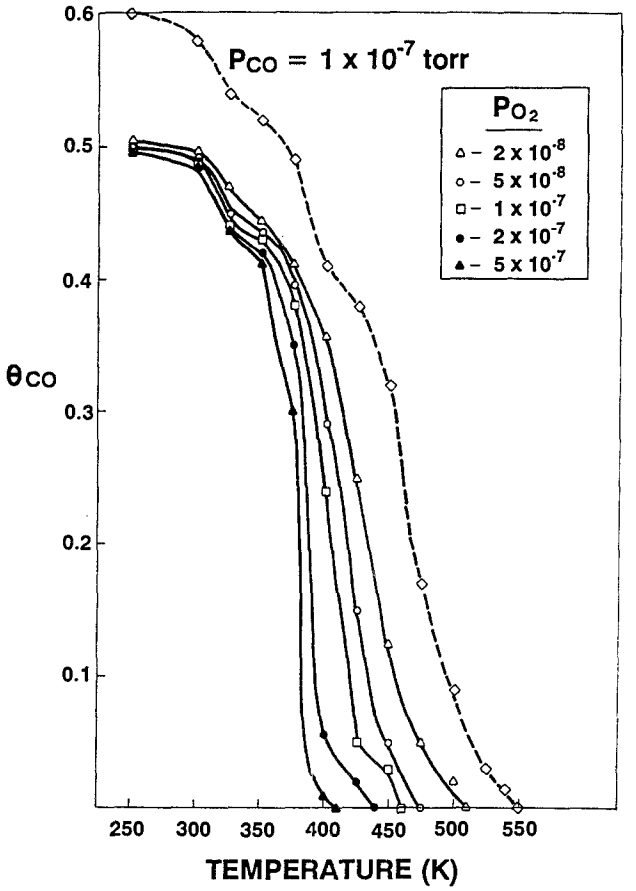

Fig. 3. Plots of overall CO coverages versus temperature during exposure to 1×10^{-7} Torr of CO (dashed trace) and during steady-state reaction with various partial pressure of O_2 (solid traces) as indicated.

Similar $\theta_{CO} - T$ plots were also obtained with fixed CO pressure (1×10^{-7} Torr) and various other O_2 pressures between 0.2 and 5×10^{-7} Torr. These data are displayed in fig. 3. While the resulting IR spectra obtained at the various O_2 pressures display similar peak frequencies and lineshapes to that shown in fig. 2A, a major difference is that the temperature at which the CO band vanishes is highly dependent upon the O_2 pressure employed. Such an observation implies that an increase in O_2 pressure lowers the CO desorption temperature. It should be noted that the depletion of CO due to CO_2 formation cannot account for the above observation because in this temperature range of CO_2 formation rate [7] is more than an order of magnitude lower than the incident CO flux. Also of interest, as displayed in fig. 3, is that the overall CO coverage at temperatures below 350 K remains constant, independent of the O_2 pressure, and is slightly lower than the saturation CO coverage. Although the spectral features of ad-

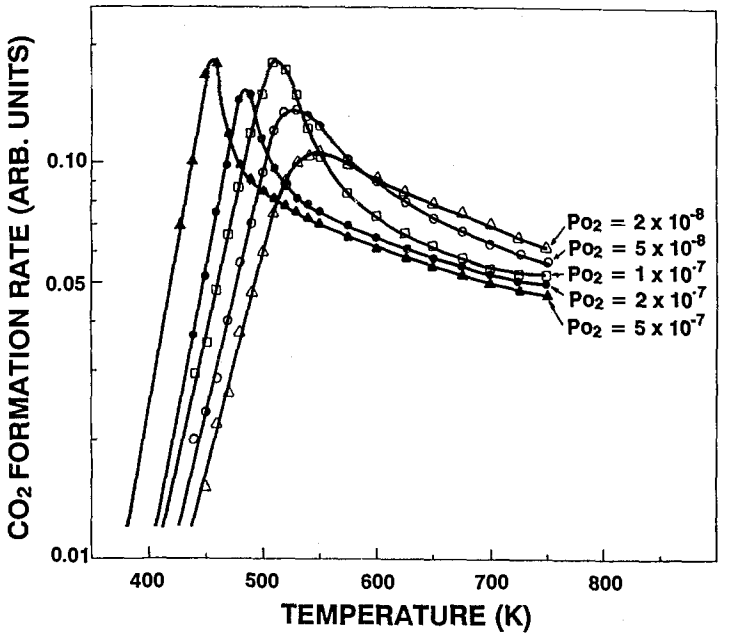

Fig. 4. Rate of CO_2 formation versus temperature for $P(CO) = 1 \times 10^{-7}$ Torr and varying $P(O_2)$ as indicated.

sorbed O_2 fall outside our accessible IR region, evidence for O_2 adsorbed on rhodium surfaces in this temperature region has been published [3–7].

Having established the relative CO coverage as a function of temperature for CO oxidation on Rh(100) at different O_2 pressures, it is of interest to examine the CO_2 formation rate under identical conditions. Figure 4 displays the CO_2 formation rates as a function of temperature for 1×10^{-7} Torr CO at different pressures of O_2. These curves display a typical volcano shape, similar to data reported previously for Rh [2,3], in which the CO_2 formation rate maximizes at a progressively higher temperature with decreasing O_2 pressure.

The observed rates of CO_2 formation displayed in fig. 4, when compared to the corresponding CO coverage plots in fig. 3, reveal that less than 1% of a monolayer of CO is present on the Rh(100) surface under conditions where the CO oxidation is maximized. Moreover, CO_2 formation rates in each case (fig. 4) do not show significant values with respect to the maximum rate until a substantial amount of adsorbed CO has been removed. These data are then consistent with the generally accepted model of this reaction [3–7] in which adsorbed CO inhibits the reaction at high coverages. Additional information is also provided by the lineshape of the IR bands shown in fig. 1A compared with the analogous bands obtained with both CO and O_2 present. The lack of any significant changes in the lineshape of CO adsorbed with O_2 in the temperature region employed here suggest that the reaction between adsorbed CO and oxygen likely takes place at the edge of CO

islands. A similar mechanism has also been proposed for CO oxidation on other single crystal surfaces [1,2]. Furthermore, these data imply that the removal of the initially adsorbed CO layer is the rate-limiting process for the CO oxidation below the temperature at which the CO_2 formation rate maximizes. At higher temperatures, where the Rh(100) surface is presumably saturated with adsorbed O_2 [3–7], a substantial drop in the CO_2 formation rate is attributed to a deficiency of adsorbed CO.

In summary, IRAS data show that the CO_2 formation rate under the reaction conditions used in this study (CO: 1×10^{-7} Torr, O_2: $0.2\text{–}5 \times 10^{-7}$ Torr) maximizes at a CO coverage of < 0.01 monolayers. Furthermore, these results indicate that CO desorption is the rate limiting process below the temperature at which the CO_2 formation rate is maximum.

Acknowledgement

We acknowledge with pleasure the support of this work by the Department of Energy, Office of Basic Energy Sciences, Division of Chemical Sciences.

References

[1] T. Engel and G. Ertl, Adv. Catal. 28 (1979) 1.
[2] T. Engel and G. Ertl, in: *The Chemical Physics of Solids Surfaces and Heterogeneous Catalysis*, eds. D.W. King and D.P. Woodruff, Vol. 4 (Elsevier Scientific Publishing Company, Amsterdam, 1982) Ch. 3.
[3] C.T. Campbell and J.M. White, J. Catal. 54 (1978) 289.
[4] Y. Kim, S.-K. Shi and J.M. White, J. Catal. 61 (1980) 374.
[5] H.-G. Lintz and T. Weisker, Appl. Surface Sci. 24 (1985) 251.
[6] W.M. Daniel and J.M. White, Int. J. Chem. Kinet. 17 (1985) 413.
[7] S.B. Schwartz, L.D. Schmidt and G.B. Fisher, J. Phys. Chem. 90 (1986) 6194.
[8] L.-W.H. Leung, J.-W. He and D.W. Goodman, in preparation.
[9] L.J. Richter, B.A. Gurney and W. Ho, J. Chem. Phys. 86 (1987) 477.
[10] B.A. Gurney, L.J. Richter, J.S. Villarrubia and W. Ho, J. Chem. Phys. 87 (1987) 6710.
[11] D.G. Castner, B.A. Sexton and G.A. Somorjai, Surface Sci. 71 (1978) 519.
[12] Y. Kim, H.C. Peebles and J.M. White, Surface Sci. 114 (1982) 363.
[13] B.N.J. Persson, F.M. Hoffmann and R. Ryberg, Phys. Rev. B 34 (1986) 2266.